Engineering Structures 154 (2018) 1–9

Contents lists available at ScienceDirect

Engineering Structures

journal homepage: www.elsevier.com/locate/engstruct

Investigation and verification on seismic behavior of precast concrete frame piers used in real bridge structures: Experimental and numerical study

Hongya Qu[b], Tiantian Li[b], Zhiqiang Wang[a,*], Hongyi Wei[a], Jiawei Shen[a], Hao Wang[a]

[a] Department of Bridge Engineering, Tongji University, Shanghai 200092, China
[b] Department of Civil, Architectural and Environmental Engineering, Missouri University of Science and Technology, 1401 N Pine St, Rolla, MO 65409, USA

ARTICLE INFO

Keywords:
Precast concrete
Segmental construction
Frame pier
Cyclic loading
Seismic performance
Groutedconnection
Finite element method

ABSTRACT

In this study, quasi-static cyclic test was conducted for three 1/3-scale specimens of different precast concrete frame pier structure systems of an urban viaduct in Shanghai, China. Various connection deployment strategies were utilized for the specimens, in order to verify these precast concrete frame piers used in the real structure. Two of the specimens were of the same cap beam design, while the third one was with tie beam. The two frame piers with cap beam had the same column-footing connection (grouted splice sleeve coupler), but the column-cap connections were grouted splice sleeve coupler and grouted corrugated duct connection, respectively. The frame pier with cast-in-place tie beam, however, only kept the grouted splice sleeve coupler for column-footing connection. The cyclic test results showed similar seismic behavior of the two specimens with cap beam, whereas the specimen with tie beam exhibited less energy dissipation capacity. This indicated that the seismic performance differences among the specimens are mainly caused by different structure systems, and the two types of the connections behave similarly with little damage. Finite element models that were optimized by considering joint region behavior and bond-slip phenomena showed good agreement with the test results.

1. Introduction

Bridge design and construction have experienced innovations and advancements in recent years, which lower overall cost, simplify construction process, and save time [1]. Bridge columns, cap beams, and bridge girders can be prefabricated in factories or near construction sites. These components are then assembled on-site using different types of connections for accelerated construction. However, connections are usually applied to critical structural locations (e.g. column-cap and column-footing joints), where plastic hinges are likely to form under strong earthquakes. Thus, studies on the bridge structures with moment-resisting connections need to be taken special care of in moderate-to-high seismic zones.

Five different types of connections were studied and used in real applications [2]. Socket connection, applied to column-footing joints, was recently utilized for highway bridges, and studies showed acceptable seismic performance [3,4]. The second type is pocket connection, and its seismic performance was also reported to be comparable to cast-in-place (CIP) structures [5]. Prestressing tendon is the third type of connection, which is commonly used in precast segmental bridge columns. Seismic behavior of these precast segmental posttensioned bridge columns was investigated experimentally, and test results showed that the segmental columns exhibit good drift capacity and ductility, and energy dissipation capability can be ensured by using energy dissipation bars [6,7]. The remaining two connection types are grouted corrugated duct connection (GCDC) and bar coupler connection, and these connections are studied in this paper. GCDC was originally developed for column-cap connections [8,9], but study of column-footing connection using GCDC was also conducted with promising results for construction [10], and good ductile performance was observed when compared with CIP systems. The bar coupler connection includes several types of proprietary mechanical bar couplers or splicing devices, one of which is grouted splice sleeve coupler (GSSC). GSSC was also studied for applications in seismic zones, including the utilization of multiple reinforcing bars, high-strength grout, and cast iron sleeve [2,11–13]. The experiments showed that specimens using GSSC and corresponding CIP structure retained equivalent strength capacity, but displacement capacity was found to be lower [14–17]. Further research studies revealed that displacement capacity can be improved by allowing debonding of reinforcing bars outside the GSSC [18]. Comparison of three specimens with various GSSC embedding locations also confirmed results of previous studies [19].

Numerical simulation was conducted to obtain better knowledge on the overall performance of the structures and connections. A two

* Corresponding author at: Department of Bridge Engineering, Tongji University, 1239 Siping Rd., Shanghai 200092, China.
E-mail address: wangzhiq@tongji.edu.cn (Z. Wang).

http://dx.doi.org/10.1016/j.engstruct.2017.10.069
Received 24 May 2017; Received in revised form 24 October 2017; Accepted 24 October 2017
Available online 03 November 2017
0141-0296/

dimensional (2-D) finite element model (FEM) was developed to simulate the precast bridge column using GCDC by modifying the elastic modulus of the reinforcing bar to consider bond-slip effect at the column-footing area [10]. Another two types of bond-slip models were proposed to explore the bond response of stainless energy dissipation bars installed in GCDC [20]. GSSC was modeled in 2-D with a nonlinear rotational spring to simulate the bond-slip effects [18,21,22].

Studies regarding the different types of connections are mainly focused on single-column piers, and those of dual-column frame piers are lacking. Only a few quasi-static cyclic tests were performed for precast dual-column frame piers with the combination of GCDC, socket and pocket connections [23,24]. Test results showed that the precast frame piers achieved good strength and ductility in comparison with CIP construction. A multi-shaking table test of a quarter-scale bridge system of two-span, three dual-column frame piers was conducted with socket and hybrid-bar-socket connections, and the maximum displacement of the precast piers was comparable with the conventional bridge [25]. State-of-practice of precast pier cap systems, including GCDC, GSSC and pocket connections, was reported by researchers and it was concluded that seismic behavior of connections was critical to system ductility [26].

This paper presents experimental and numerical study of three 1/3-scale specimens of precast bridge substructures (dual-column frame pier) that are assembled with different connections (GCDC and GSSC) under lateral quasi-static cyclic load. The specimens are based on the precast frame piers that are utilized in urban viaducts of highway S6 in Shanghai, China. The viaducts also retain the precast bridge decks, and the frame piers are commonly used as a substructure for these decks, which led to the choice of such structure system. Since it is permitted by the load capacity of the cranes, the columns can remain the integrity without being divided into several segments, which also facilitates the construction process. The two types of connections are proven by the contractors to be more convenient than others in terms of construction. For example, it avoids the post-tensioning procedure, if the precast hollow section piers are used. Moreover, the deployment strategies of these connections of the frame piers (GSSC at both column ends, and combined GSSC and GCDC at each end) have never been used and studied, and therefore the seismic behavior of these frame piers is unknown and needed to be investigated and verified.

Study on seismic behavior of six precast single-column piers with different connection details was also conducted by the present authors [27], including GSSC, GCDC and posttensioned connections. The columns with GSSC and GCDC were designed the same as those of frame pier specimens studied in this paper, and their seismic performances were compared with the CIP benchmark. It was concluded that these columns with GSSC and GCDC were emulative of CIP reinforced concrete columns if high-strength grout was used. Therefore, the seismic behavior of precast bridge frame piers is investigated without a CIP reference in this study. Two of the specimens are with cap beams and share exactly the same design except for the connections, while the third one uses CIP tie beam design. The test results were compared to further understand the seismic behavior of the frame piers. 2-D FEMs were also developed with different approaches to optimize the accuracy of simulation. The bond-slip phenomena were simulated by considering 6% inactive length of the skin reinforcements at both ends of the columns, and the beam-column joint region behavior unique to frame piers was also considered.

2. Test setup

2.1. Specimens

The urban viaducts of highway S6 in Shanghai possess a total length of 11.8 km. It provides a crucial passage and eases the pressure of the city transportation. These continuous bridges that were constructed along the highway are 30 m long for each span (Fig. 1). In order to accommodate the traffic and design requirement, all the three precast frame pier designs of the tested specimens are used. The bridges with box-girders are more suitable for the piers with tie beam design, while the ones with T-girders are better supported with cap beam design. Moreover, GCDCs require long anchoring length ($>$ 25 times the rebar diameter), while GSSC needs shorter length (8–10 times the rebar diameter). The cap beams at different locations do not maintain the same height, and GSSC is thus used where the cap beam height cannot meet the anchoring requirement of GCDC, while GCDC is implemented for those with enough height in terms of economic efficiency. In addition, an ongoing study of the durability of these connections and designs also requires all the bridge pier types to be constructed and monitored to serve this purpose. These three types of the precast frame pier specimens are tested for verification purposes, and each one has a unique connection deployment, but they are with the same column dimension and mild reinforcement arrangement.

The concrete material used is C40, and its nominal uniaxial compressive strength and modulus of elasticity are 26.8 MPa and 3.25×10^4 MPa, respectively. To determine actual concrete strength, nine 150 mm concrete cubes made from the same concrete sample are modeled and standard-cured for 28 days. The average compressive strength of the nine cubes is 33.5 MPa, and the modulus of elasticity is 3.3×10^4 MPa. For mild reinforcement, hot-rolled plain bar with nominal yield strength of 235 MPa (HPB235) and hot-rolled ribbed bar with nominal yield strengths of 335 MPa and 400 MPa (HRB335 and HRB400) are used. Nominal moduli of elasticity are 2.1×10^5 MPa for HPB235 and 2.0×10^5 MPa for HRB335 and HRB400. Based on coupon tests of the three specimens from each type of steel, the average measured yield strengths of HPB235, HRB335 and HRB400 are 243 MPa, 390 MPa and 432 MPa, and the averaged ultimate strengths are 404 MPa, 499 MPa and 601 MPa. High-strength grout is used for the connections, and nine 70 mm cubes are modeled and standard-cured with an average 28-day compressive strength of 104 MPa.

The columns in all three specimens are 3050 mm tall with the rectangular cross-section of 500 mm × 530 mm (Fig. 2). In order to keep the same loading height, the footing of specimen #3 is raised from 600 mm to 750 mm to compensate the height decrease due to the tie beam design. Detailed reinforcement arrangements for columns are shown in Fig. 3(a)–(c). The longitudinal reinforcements consist of 20 mm-diameter HRB400s and 8 mm-diameter HPB235s that is referred to as skin reinforcement for crack prevention. The hoops are 8 mm-diameter HPB235s and the ties are 6 mm-diameter HPB235s, and both are spaced at 50 mm. For locations where GSSC and GCDC are embedded, stirrups and ties are all 8 mm-diameter HPB235s spaced at 45 mm. Reinforcement arrangement for the tie beam is shown in Fig. 3(d). The longitudinal reinforcements consist of 10 mm- and 12 mm-diameter HRB335s. The hoops and ties are 8 mm- and 6 mm-diameter HPB235s with a clear spacing of 60 mm.

GSSC is a hollow steel bar coupler that connects the rebars from each component, while GCDC is a flexible corrugated metal tube that provides the guidance for the protruding rebar of one component to be inserted into another component. In terms of the placement of connections, GSSCs are embedded in the footing and cap beam of specimen #2, while GSSCs are replaced by GCDCs in the cap beam for specimen #1. Specimen #3, however, only has GSSC placed inside the lower ends of the columns, and no connections are used at the upper ends due to the CIP tie beam. The lengths of GSSCs and GCDCs are 360 mm and 700 mm, and the nominal diameters are 66.5 mm and 40 mm, respectively. The details of the GSSC and GCDC used in the specimens are shown in Fig. 4.

The fabrication processes of specimens #1 and #2 are similar, and the only difference between the two is the protruding length of the 20 mm-diameter longitudinal rebars (175 mm for GSSC and 680 mm for GCDC). The precast segments include pier cap, column, and footing, as shown in Fig. 5(a)–(c). After the completion of concrete curing, the columns of each specimen are mounted on the footing by inserting the

Fig. 1. Actual precast frame pier assembly of highway S6.

protruding rebars into the corresponding connections. A 2 cm gap between the footing and columns is kept, and formwork is then established around the gap (Fig. 5d). By holding the columns in position, high-strength mortar is grouted into the connections until it is saturated, and the inlets and outlets are instantly sealed afterwards (Fig. 5e). By repeating the procedure for the column-cap connections, the piers can thus be promptly constructed. For specimen #3, after connecting the columns and footing using the same procedure, the tie beam is then cast in place (Fig. 5f–i). Unfortunately, there exist no reliable connection strategies for the tie beams to be connected to the columns, but limited disturbance is caused by the CIP tie beam thanks to the smaller dimension and more localized placement. Among all the bridges of highway S6, the ones with tie beam design are less than 10%, which has minor impact for the overall accelerated construction process.

2.2. Test program

The frame piers are subjected to quasi-static unidirectional cyclic loading with the actuator located at 4 m above the ground. The actuator has built-in load cell and displacement sensor at the load stub, and its maximum load capacity and travel distance are 1500 kN and ± 250 mm. The specimens are tested with a pre-defined loading protocol under displacement control, as shown in Fig. 6. To be more specific, 17 displacement levels are performed, and three full loading cycles are conducted for each level. Multiple hydraulic jacks are implemented on the top surface of the cap beam (specimens #1 and #2) and of the columns (specimen #3) applying constant vertical loads (560 kN per column) during the testing procedure to simulate the weight of the superstructure.

In order to obtain curvature variation at critical locations where plastic hinges may occur, displacement sensors are installed at the lower end of each column. A pair of sensors at the same height is considered as a group. There are three groups for each column in all specimens, and they are all mounted on the column surfaces that are perpendicular to the load direction. For these sensor groups, they are measuring the relative displacement variations at 75 mm, 225 mm, and 650 mm above the column-footing interface. Strain gauges are attached on the 20 mm-diameter longitudinal reinforcements and the outer surfaces of GSSCs. These strain gauges are placed near the column-footing region, and the exact locations are given in Fig. 7.

3. Interpretation and comparison of test results

The performance level of bridge can be divided into five stages, which includes (1) cracking, (2) yielding, (3) initiation of local mechanism, (4) full development of local mechanism, and (5) strength degradation [28]. Fig. 8 shows the damage progression of the column bottom of specimen #1 at all five stages, and all specimens are of similar results.

Level 1 happened when the maximum displacement of the column top reached 10 mm (0.31% drift ratio), and there was onset of hairline cracks (less than 0.1 mm wide) that closed up when the specimens were re-centered. Level 2 initiated at 15 mm (0.46% drift ratio), cracks were widened (< 0.2 mm) and interconnected with each other across the surfaces. Two ends of the tie beam in specimen #3 also began to develop visible cracks. Longitudinal rebars started to yield at the displacement of 14 mm. Level 3 was between 60 mm and 80 mm

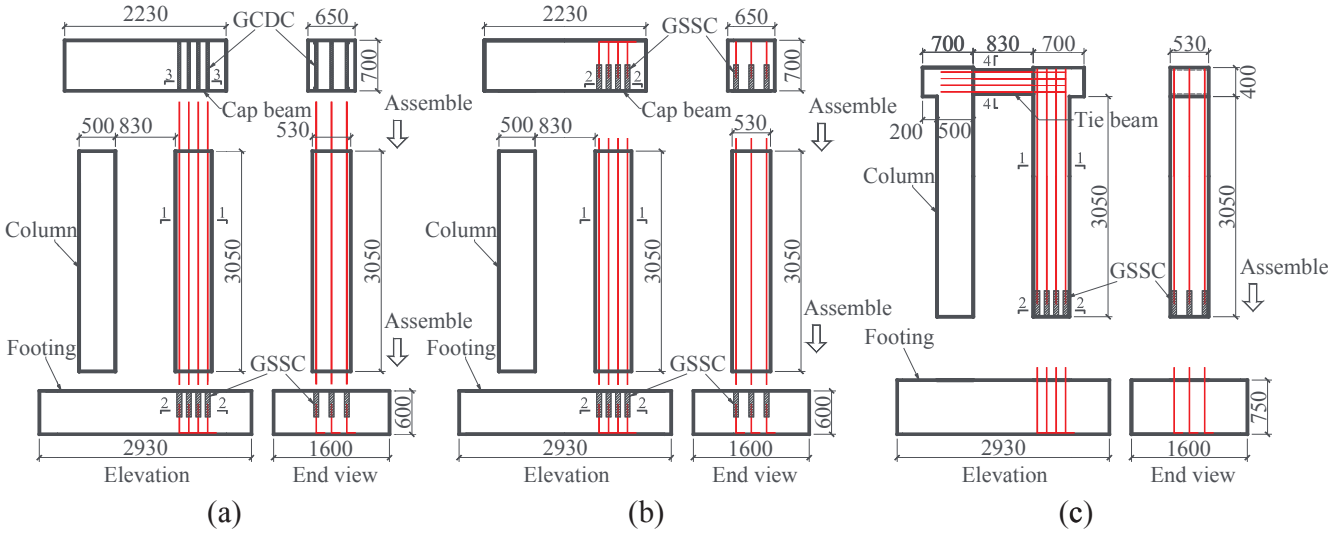

Fig. 2. Dimensional and structural details of frame pier specimens: (a) Specimen #1; (b) Specimen #2; (c) Specimen #3.

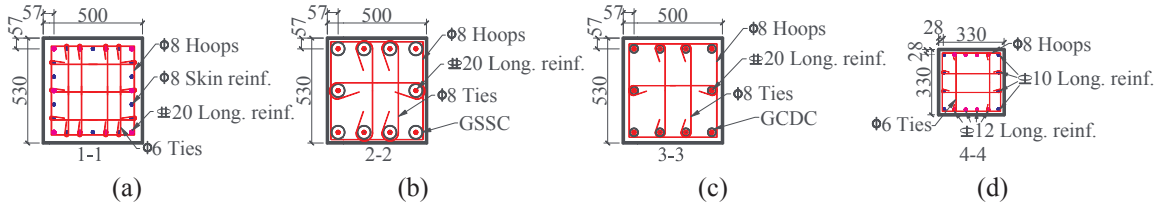

Fig. 3. Reinforcment arrangments and connection details: (a) Column; (b) GSSC; (c) GCDC; (d) Tie beam.

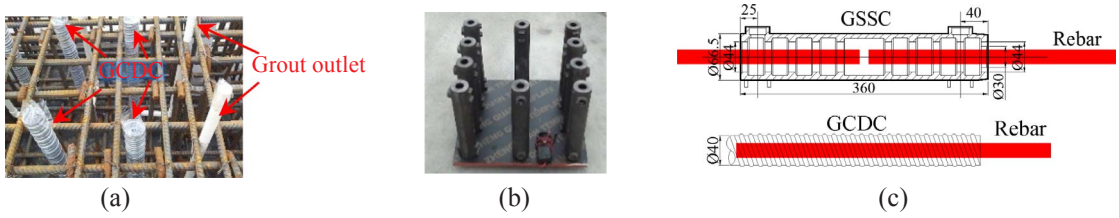

Fig. 4. Details of GCDC and GSSC: (a) GCDC; (b) GSSC; (c) Sketch of GCDC and GSSC.

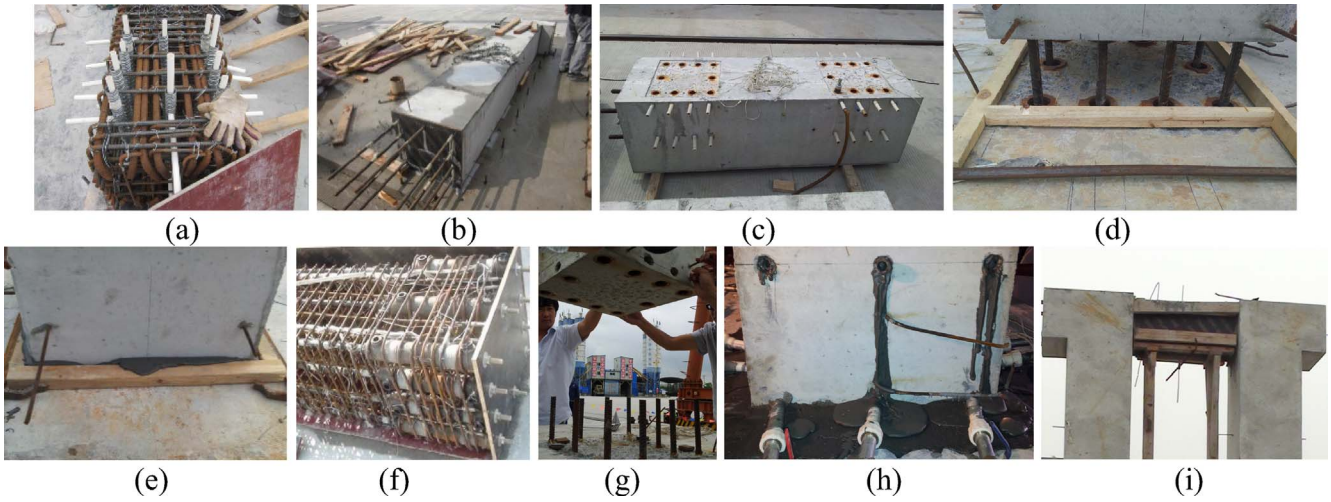

Fig. 5. Photographs during construction: (a) Reinforcement cage of cap beam for specimen #1; (b) precast column after removing mold (specimen #1); (c) precast cap beam of specimen #2; (d) assembly of column to footing of specimen #2; (e) column-footing grouting of specimen #2 (f) column reinforcement cage of specimen #3; (g) assembly of column to footing of specimen #3; (h) grouting of specimen #3; (i) on-site casting of tie beam.

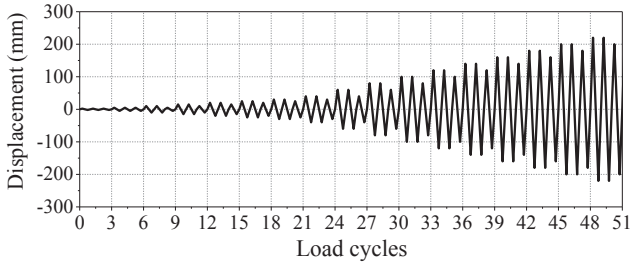

Fig. 6. Loading protocol.

displacement level, and there was onset of concrete spalling at both ends of the columns for specimens #1 and #2, while spalling areas at the upper ends of the columns were replaced by the two ends of tie beam for specimen #3. The width of the cracks reached up to 1 mm, but the number of cracks had no obvious increase. Level 4 appeared at the displacement level of 120 mm, and the length of concrete spalling region at the column top and bottom extended to 200 mm. Part of the longitudinal rebars buckled, but none of them fractured. Tie beam of specimen #3 also experienced concrete spalling increase within the 200 mm region. Fracture of longitudinal rebars and crush of core concrete indicated the presence of level 5, and test was terminated at this point.

The final crack patterns of each specimen are shown in Fig. 9(a). Similar patterns are found for specimens #1 and #2, but specimen #1 has more severe damage at the column top, which is caused by the connection difference. Plastic hinges formed at both ends of the tie beam instead of column top for specimen #3. The actual damage comparison of the pier caps and the tie beam is given in Fig. 9(b), and it clearly shows the different failure mechanisms. Note that only a few longitudinal reinforcements are fractured, but no connections are damaged.

The load-displacement relationships of all specimens are shown in Fig. 10, and all hysteresis loops cover good amount of areas, indicating effective energy dissipation capability. Pinching effect is present at the later stage of the test, which is mainly caused by the presence of bond-slip behavior of the reinforcements.

The comparison of the backbone curves extracted from the hysteretic behaviors of all specimens is shown in Fig. 11. All curves exhibit constant stiffness within a short displacement range, and stiffness degradation is then followed. As expected, specimen #3 possesses smaller structural strength, and the other two specimens are similar.

Based on the hysteretic behaviors of the specimens, further analysis can be performed. Ductility (μ) is defined as the ratio of ultimate displacement (Δ_u) and effective yield displacement (Δ_y). Δ_u is the

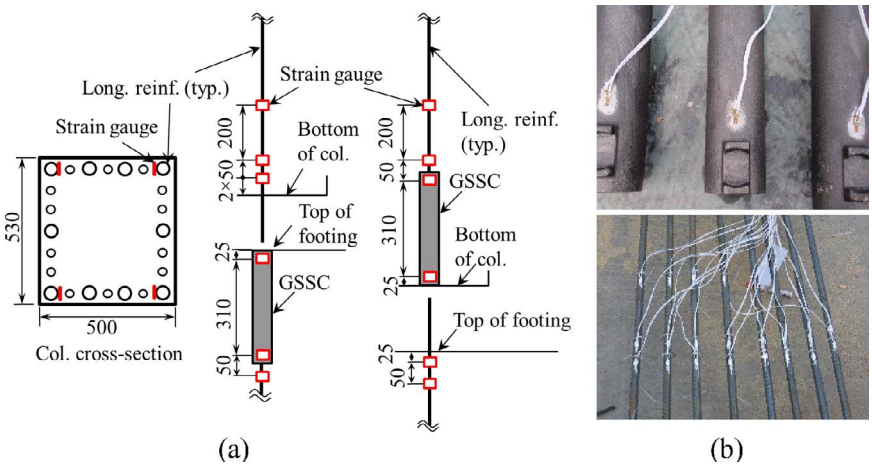

Fig. 7. Strain gauge deployment: (a) Sketch (unit: mm); (b) Actual attachment.

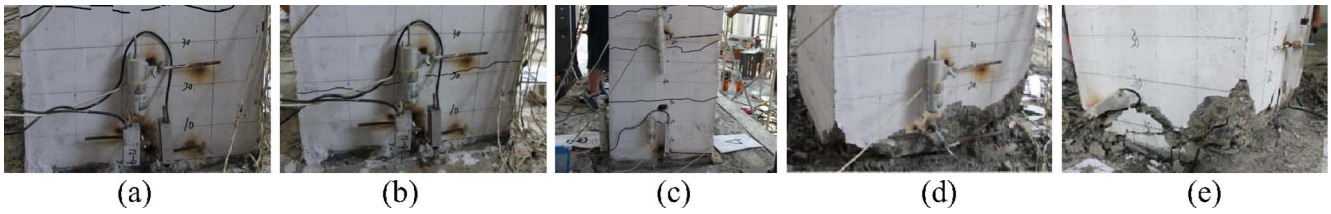

Fig. 8. Damage development at five performance stages of specimen #1: (a) Stage 1; (b) Stage 2; (c) Stage 3; (d) Stage 4; (e) Stage 5.

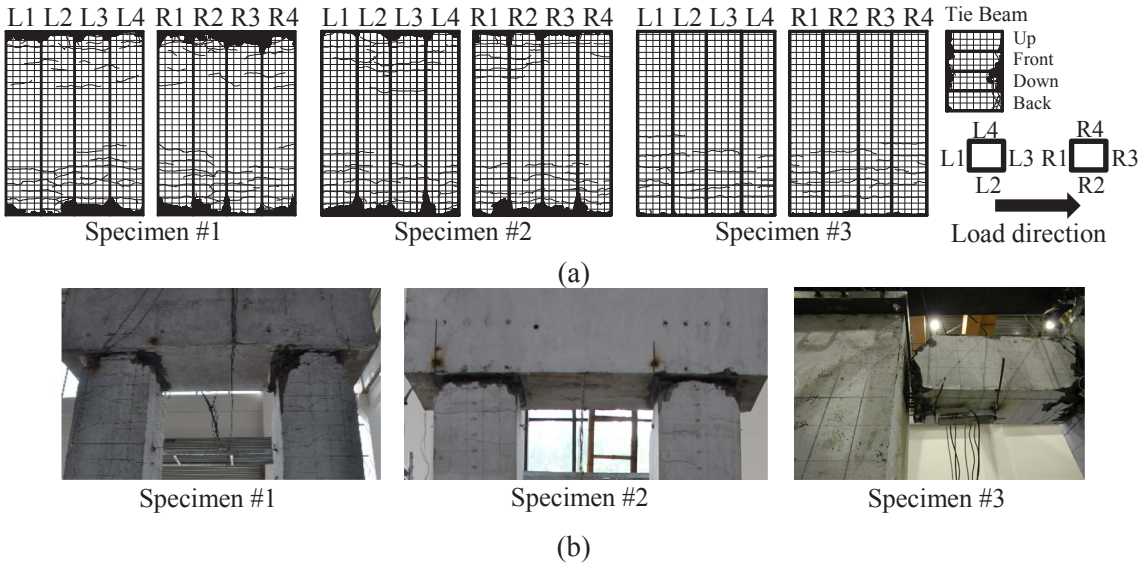

Fig. 9. Crack pattern and concrete spalling of the columns and tie beam at the final stage: (a) Sketch; (b) Actual damage.

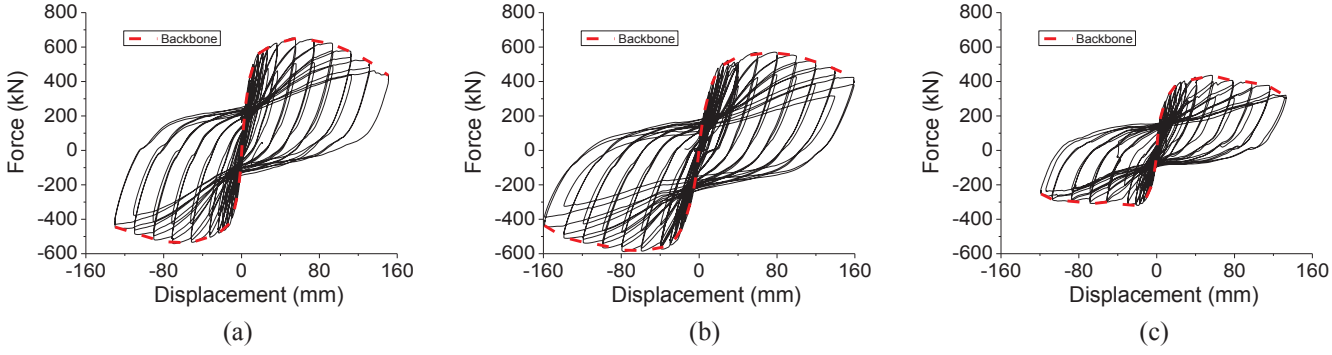

Fig. 10. Load-displacement relationship: (a) Specimen #1; (b) Specimen #2; (c) Specimen #3.

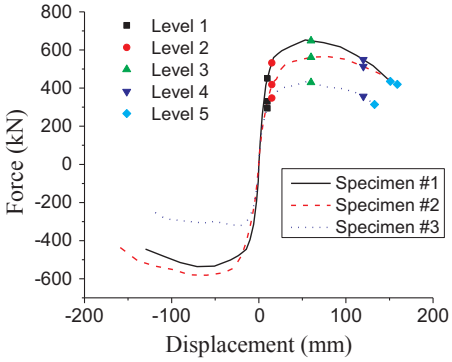

Fig. 11. Backbone curves of all specimens.

Table 1
Ductility of the specimens.

	Specimen #1	Specimen #2	Specimen #3
Δ_y (mm)	16.11	16.50	17.01
Δ_u (mm)	118.16	117.56	116.18
μ	7.33	7.12	6.83

displacement where the strength decreases to 85% of the ultimate strength, and Δ_y is determined by the method proposed by Park [29]. Ductility values are calculated and presented in Table 1 for comparison, and specimen #3 retains a slightly smaller value than the other two.

Accumulated energy dissipation is the summation of the area covered by each hysteresis loop, which is used to evaluate the energy a structure is able to dissipate. Fig. 12(a) shows the accumulated energy dissipation of all specimens at each displacement level. All specimens exhibit considerable energy dissipation capacity, but specimen #3 is still smaller than the other two. As the tie beam of specimen #3 becomes the energy dissipation component, its smaller cross-section results in less capacity. Stiffness degradation is analyzed through the ratio of effective stiffness (K_{eff}) to initial stiffness (K_0) at different displacement levels. The initial stiffness values of the three specimens are similar (67.97, 66.60 and 70.14 kN/mm), but specimen #3 has smaller strength progression which in turn results in smaller effective stiffness (Fig. 12b). All the values of K_{eff}/K_0 tend to decrease rapidly within the displacement level of 40 mm and slow down after concrete is damaged. Residual displacement index (RDI) is an important indicator for assessing the self-centering capability of the structure. It is defined as the ratio of residual displacement to yield displacement: RDI = Δ_r/Δ_y. Fig. 12(c) shows the RDI values of the three specimens at different displacement levels, and differences among these three are insignificant.

Curvature is calculated through the displacement sensors mounted on both sides of the columns at different heights. Fig. 13 gives the curvature developments at previously defined four performance levels for the specimens. All three specimens have almost identical results, and the magnitudes decrease rapidly along the column heights. Thus, the damage developments of all three specimens at the column bottom regions are similar, and the plastic hinge region is limited to the length of 0.2 m.

Strain distributions at the connection regions are shown in Fig. 14, and location 0.0 m represents the column-footing interface. Strain values of the connections experience little increase, which confirms that little damages have occurred at the connections. However, those of the rebars close to the connections increase significantly, indicating that severe bond-slip behavior has occurred. Such bond-slip behavior quickly vanishes as the distance from the connections becomes larger.

4. Numerical simulation and evaluation

The FEMs are developed by OpenSees [30], and three different modeling approaches are used (Fig. 15). The material of the confined concrete used is Concrete07 for more detailed and accurate simulation, while that of unconfined concrete is Concrete01. Rebars are modeled with the material of Reinforcing Steel considering buckling, fatigue and strength reduction.

Fiber elements, specifically force-based beam-column (B-C) elements, are used in three major components (column, GSSC, and tie beam), of which plastic hinges are likely to form. Core concrete of the columns is meshed into 20 × 20 squares, while the mesh of tie beam has 10 × 10 squares. Concrete cover is simply divided into four elements along each edge. GSSC is simulated with Reinforcing Steel material, but it has the diameter of the connection. Elastic B-C elements are used to model cap beams for both calculation efficiency and high structural stiffness. The frame piers are different from the single-column pier structure, in terms of the cap beam- or tie beam-column interaction. Thus, in addition to the application of fiber elements, the joint regions of specimens #2 and #3 are further analyzed with VecTor2 [31]. Pinching4 material is applied to the joint region for the FEMs with four stress-strain floating points, based on the results of VecTor2 under monotonic loading (Fig. 16).

Specimen #1 only uses the fiber element with the given materials without considering any other factors, and therefore it is the simplest approach. In terms of the parameters for strength reduction of the Coffin-Manson model, the optimal values are found as $C_f = 0.6$, $\alpha = 0.506$ and $C_d = 0.5$ through parametric study. The comparison of the hysteresis curves is shown in Fig. 17(a), and the unload stiffness exhibits considerable differences between the test and simulation results. Pinching effect of the numerical model is not obvious. From the comparison of backbone curves in Fig. 17(b), initial stiffness of the numerical model is larger, since bond-slip effect is not considered in this case.

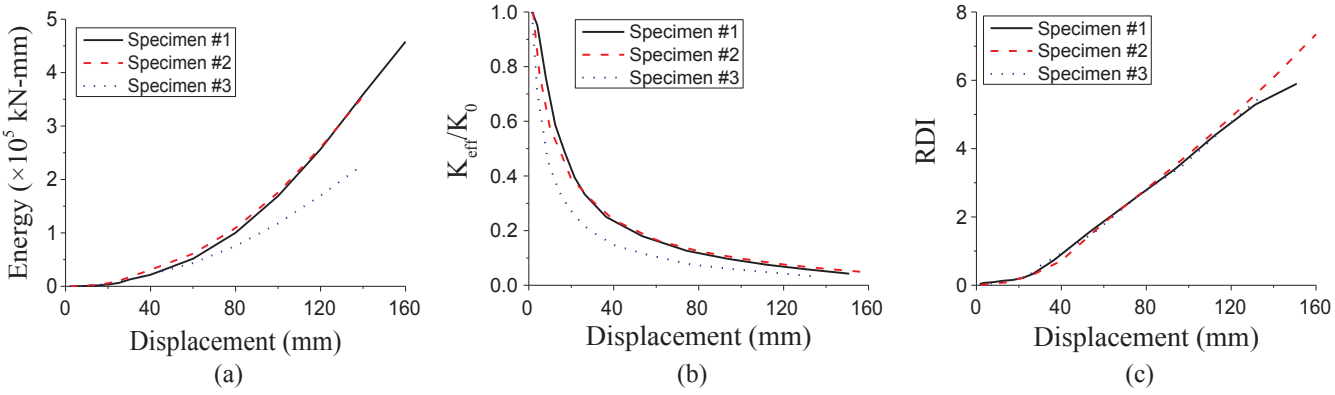

Fig. 12. Comparison of structural parameters: (a) Accumulated energy dissipation; (b) Normalized effective stiffness; (c) Residual displacement index.

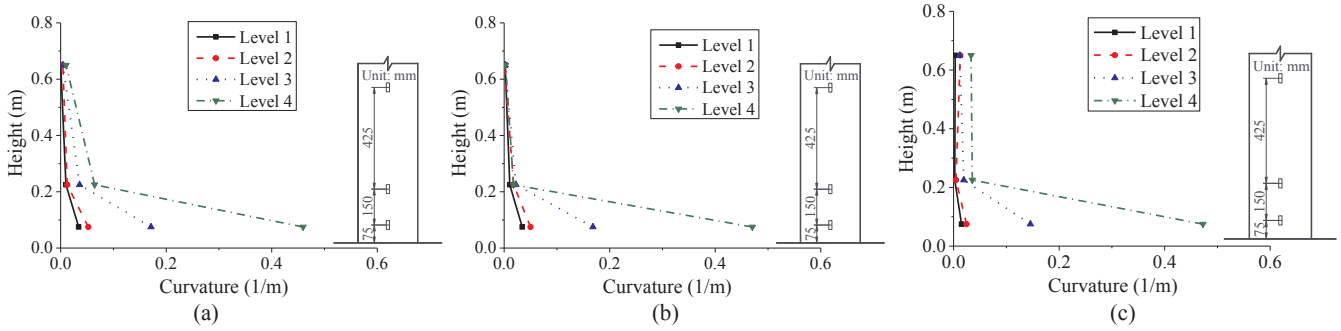

Fig. 13. Comporison of curvature at column bottom area: (a) Specimen #1; (b) Specimen #2; (c) Specimen #3.

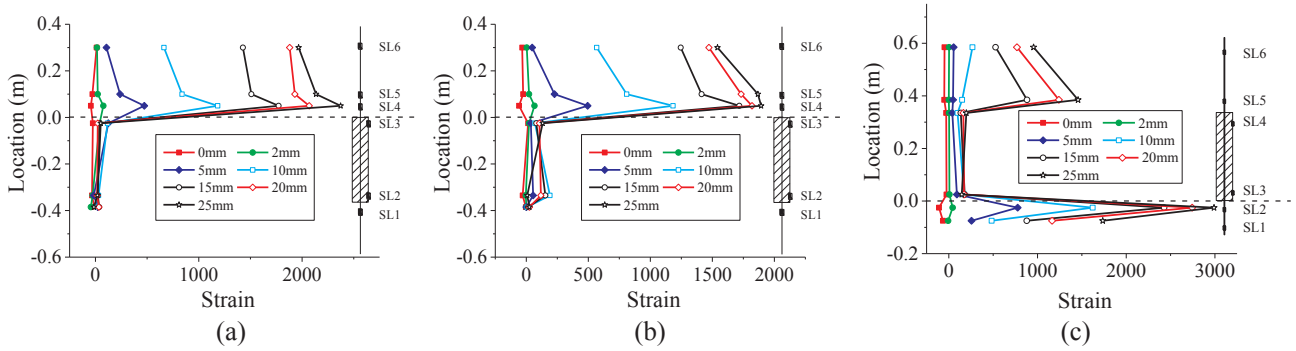

Fig. 14. Comparison of strain distribution: (a) Specimen #1; (b) Specimen #2; (c) Specimen #3.

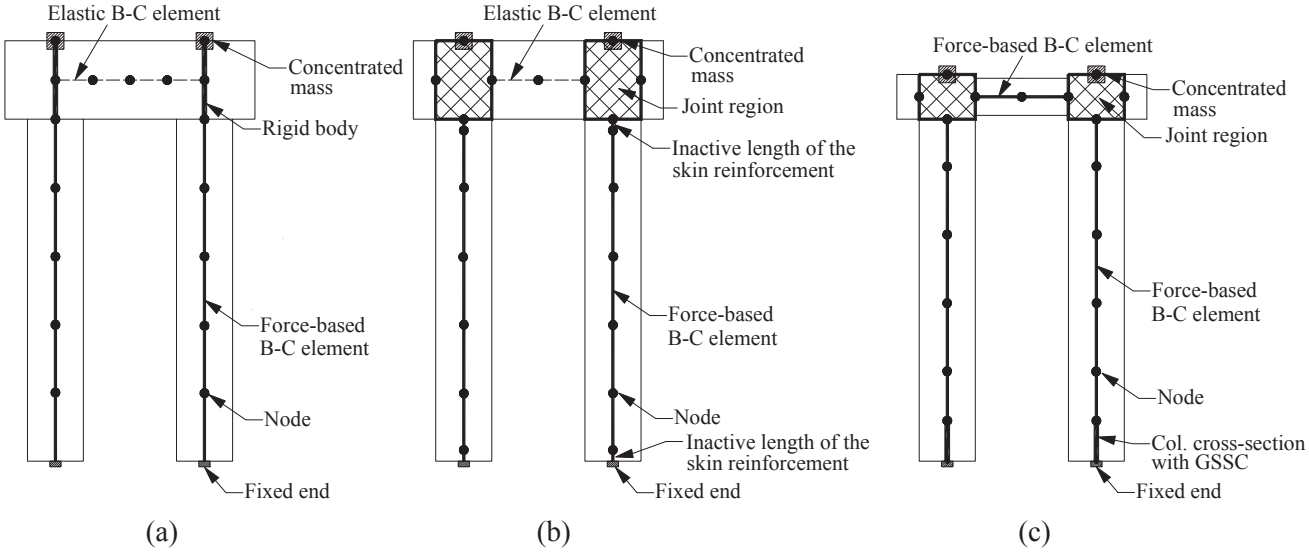

Fig. 15. FEMs of all specimens: (a) Specimen #1; (b) Specimen #2; (c) Specimen #3.

Simulation of specimen #2 is further refined by considering both the inactive skin reinforcement lengths at two column ends and the beam-column joint region behaviors. The inactive length of the skin reinforcement is optimized to be 180 mm (6% of column height). Joint region behavior is obtained based on the shear stress and strain curve from VecTor2 as illustrated previously. Improvements can thus be found for the unload stiffness and pinching effect, and the backbone curves also show good agreement (Fig. 18).

In addition to the modeling approaches of specimen #2, specimen #3 has the GSSC placed within the columns. Therefore, the effect of GSSC has to be taken into consideration. GSSCs are modeled using Reinforcing Steel material with the diameter of the GSSC. The size of the joint regions is 530 × 500 × 400 mm for the tie beam, and it is shown in Fig. 19 that excellent agreements are found in every aspect of the hysteresis and backbone curves.

5. Conclusions

Three different designs of precast concrete frame pier specimens are studied both experimentally and numerically. These specimens are based on real bridge applications, and the study is intended to investigate and verify the seismic behavior of the structures. Based on the study, the following conclusions can be drawn:

- The seismic behaviors of specimens #1 and #2 are similar, and the bond-slip phenomena in all specimens are observed in later stage of the test, which indicates that the two types of connections are of equivalent performance. Specimen #3 shows lower energy

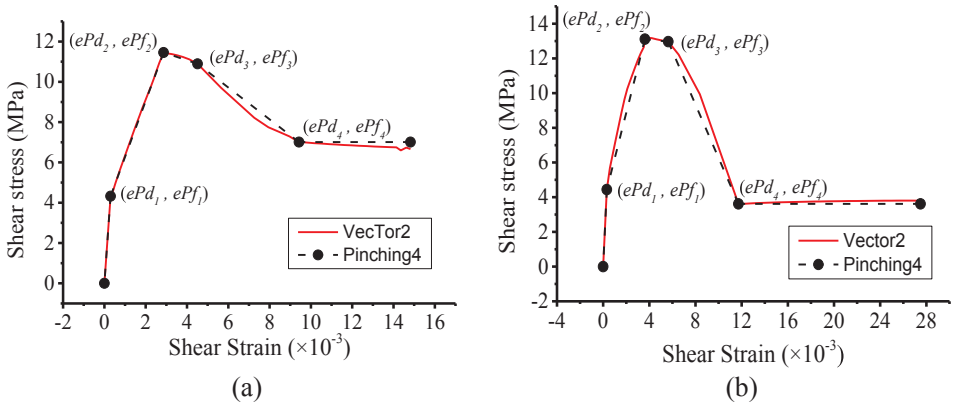

Fig. 16. Definition of Pinching4 material: (a) Specimen #2; (b) Specimen #3.

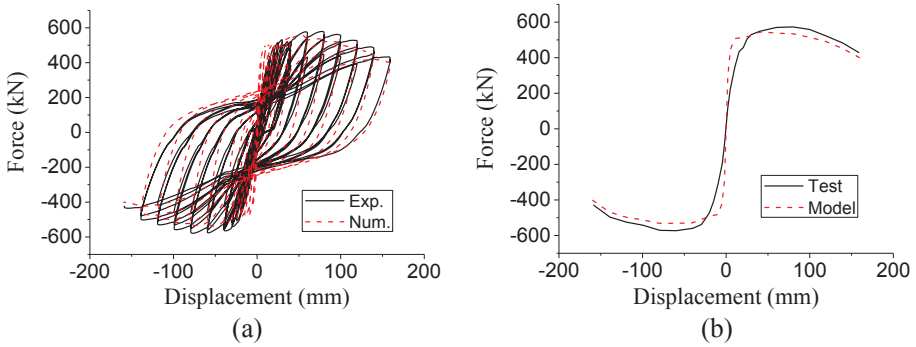

Fig. 17. Comparison of numerical and experimental results (Specimen #1): (a) Hysteretic behavior; (b) Backbone curve.

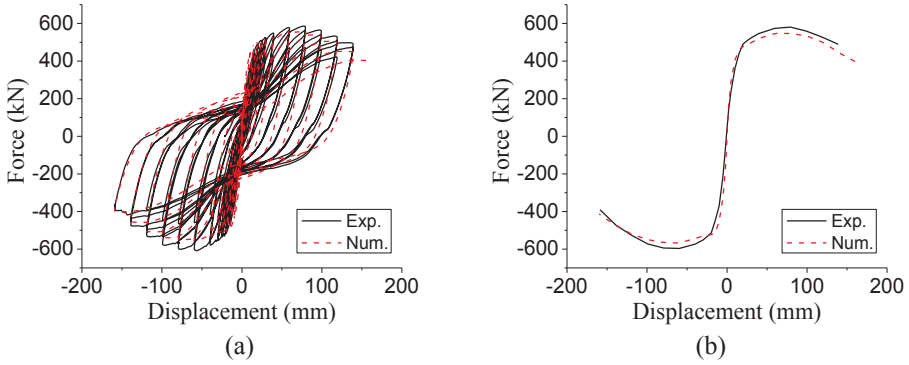

Fig. 18. Comparison of numerical and experimental results (Specimen #2): (a) Hysteretic behavior; (b) Backbone curve.

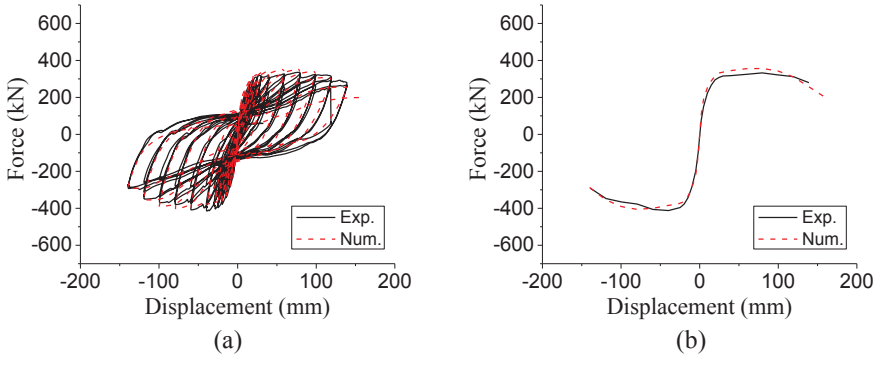

Fig. 19. Comparison of numerical and experimental results (Specimen #3): (a) Hysteretic behavior; (b) Backbone curve.

dissipation capability than the other two, which is mainly caused by the design difference.

- In addition, the energy dissipation, stiffness ratio, and residual displacement are almost identical for specimens #1 and #2, while specimen #3 retains lower values in the first two indices but similar level of residual displacement.
- The columns of specimen #3 experience little damage at the top, which is mainly taken by the tie beam. Thus, the energy dissipation capacity of the columns is not fully exerted. In other words, the overall seismic performance of the frame pier solely with tie beam is not as good as the cap beam structure, and therefore more attention needs to be paid.

- Bond-slip behavior is obvious at locations close to the connections. The connections do not experience significant strain increase despite of the embedded locations, indicating that the connections are able to maintain good integrity.
- The inactive length of the skin reinforcement applied to consider bond-slip behavior is optimized to be 6% of the column height, which in turn reduces the initial stiffness and improves simulation results. The unique behavior of beam-column joint regions for frame piers is simulated by implementing Pinching4 material, and it also effectively improves the accuracy of the FEM. GSSC modeled using the Reinforcing Steel material with enlarged diameter is proved to be feasible for FEMs.

Acknowledgement

This work was supported by the National Science Foundation of China [grant numbers 51178350 and 51378386]; Science and Technology Commission of Shanghai Municipality [grant number 13231200800].

References

[1] Brenes FJ, Wood SL, Kreger ME. Anchorage requirements for grouted vertical-duct connectors in precast cap systems: a summary. Center for Transportation Research, Project Summary Report 0–4176, Austin, TX. 2006 Jan.
[2] Marsh ML. Application of accelerated bridge construction connections in moderate-to-high seismic regions. Transportation Research Board. 2011.
[3] Khaleghi B, Schultz E, Seguirant S, Marsh L, Haraldsson O, Eberhard M, et al. Accelerated bridge construction in Washington State. PCI J 2012;57(4):34–49.
[4] Haraldsson OS, Janes TM, Eberhard MO, Stanton JF. Seismic resistance of socket connection between footing and precast column. J Bridge Eng 2013 Aug 15;18(9):910–9.
[5] Matsumoto EE. Emulative precast bent cap connections for seismic regions: Component tests—Cap pocket full ductility specimen (unit 3). ECS Rep. No. ECS-CSUS-2009-03, California State Univ., Sacramento, CA. 2009.
[6] Ou YC, Wang PH, Tsai MS, Chang KC, Lee GC. Large-scale experimental study of precast segmental unbonded posttensioned concrete bridge columns for seismic regions. J Struct Eng 2009 Sep 18;136(3):255–64.
[7] Bu ZY, Ou YC, Song JW, Zhang NS, Lee GC. Cyclic loading test of unbonded and bonded posttensioned precast segmental bridge columns with circular section. J Bridge Eng 2015 Jun 30;21(2):04015043.
[8] Matsumoto EE. Emulative precast bent cap connections for seismic regions: Component tests—Grouted duct specimen (unit 2). ECS Rep. No. ECS-CSUS-2009-02, California State Univ., Sacramento, CA. 2009.
[9] Pang JB, Eberhard MO, Stanton JF. Large-bar connection for precast bridge bents in seismic regions. J Bridge Eng 2009 Oct 12;15(3):231–9.
[10] Tazarv M, Saiidi MS. UHPC-filled duct connections for accelerated bridge construction of RC columns in high seismic zones. Eng Struct 2015 Sep;15(99):413–22.
[11] Jansson PO. Evaluation of grout-filled mechanical splices for precast concrete construction. 2008 May.
[12] Rowell SP, Grey CE, Woodson SC, Hager KP. High strain-rate testing of mechanical couplers. Vicksburg MS: Engineer Research and Development Center; 2009 Sep.
[13] Haber ZB, Saiidi MS, Sanders DH. Behavior and simplified modeling of mechanical reinforcing bar splices. ACI Struct J 2015 Mar 1;112(2):179.
[14] Tazarv M. Next generation of bridge columns for accelerated bridge construction in high seismic zones. Reno: University of Nevada; 2014.
[15] Aida H, Tanimura Y, Tadokoro T, Takimoto K. Cyclic loading experiment of precast columns of railway rigid-frame viaduct installed with NMB splice sleeves. Proc Japan Concrete Inst 2005;27(2):613–8.
[16] Haber ZB, Saiidi MS, Sanders DH. Seismic performance of precast columns with mechanically spliced column-footing connections. ACI Struct J 2014 May 1;111(3):639.
[17] Ameli MJ, Parks JE, Brown DN, Pantelides CP. Seismic evaluation of grouted splice sleeve connections for reinforced precast concrete column-to-cap beam joints in accelerated bridge construction. PCI J 2015 Mar 1;60(2):80–103.
[18] Wehbe NI, Saiidi MS, Sanders DH. Seismic performance of rectangular bridge columns with moderate confinement. Struct J 1999 Mar 1;96(2):248–58.
[19] Ameli MJ, Brown DN, Parks JE, Pantelides CP. Seismic column-to-footing connections using grouted splice sleeves. ACI Struct J 2016 Sep 1;113(5):1021.
[20] Zhou Y, Ou YC, Lee GC. Bond-slip responses of stainless reinforcing bars in grouted ducts. Eng Struct 2017 Jun;15(141):651–65.
[21] Haber ZB. Precast column-footing connections for accelerated bridge construction in seismic zones. Reno: University of Nevada; 2013.
[22] Ameli MJ, Pantelides CP. Seismic analysis of precast concrete bridge columns connected with grouted splice sleeve connectors. J Struct Eng 2016 Sep;19:04016176.
[23] Mashal M, Palermo A. Experimental testing of emulative fully precast concrete bridge bent in seismic regions.
[24] Mehrsoroush A, Saiidi MS. Cyclic response of precast bridge piers with novel column-base pipe pins and pocket cap beam connections. J Bridge Eng 2016 Jan 4;21(4):04015080.
[25] Thonstad T, Mantawy IM, Stanton JF, Eberhard MO, Sanders DH. Shaking table performance of a new bridge system with pretensioned rocking columns. J Bridge Eng 2016 Jan 4;21(4):04015079.
[26] Tobolski MJ, Ralls ML, Matsumoto EE, Restrepo JI. State-of-practice of precast bent cap systems. In Structures Congress 2006: Structural Engineering and Public Safety. 2006:1–10.
[27] Wang Z, Qu H, Li T, Wei H, Wang H, Duan H, Jiang H. Quasi-static cyclic tests of precast bridge columns with different connection details for high seismic zones. Unpublished results.
[28] Hose YD, Seible F. Performance evaluation database for concrete bridge components and systems under simulated seismic loads. Pacific Earthquake Engineering Research Center. 1999.
[29] Park R, Paulay T. Strength and ductility of concrete substructures of bridges. Transit New Zealand Road Res Unit Bull 1990;84(1):14–29.
[30] Mckenna FT. Object-oriented finite element programming: frameworks for analysis, algorithms and parallel computing. Berkeley: University of California; 1997 Jan 1.
[31] Vecchio FJ. VecTor Analysis Group: Performance assessment of concrete structures advanced modelling and forensic analysis. [cited 11 May 2017]. Available from: http://www.civ.utoronto.ca/vector.